

## Temporal-spatial dynamics of vegetation variation on non-point source nutrient pollution

Wei Ouyang<sup>a,b,\*</sup>, Xuelei Wang<sup>c</sup>, Fanghua Hao<sup>a</sup>, R. Srinivasan<sup>d</sup>

<sup>a</sup> School of Environment, State Key Laboratory of Water Environment Simulation, Beijing Normal University, Beijing 100875, China

<sup>b</sup> International Institute for Geo-Information Science and Earth Observation (ITC), Hengelosestraat 99, P.O. Box 6, Enschede 7500 AA, The Netherlands

<sup>c</sup> School of Geography, State Key Laboratory of Remote Sensing Science, Beijing Normal University, Beijing 100875, China

<sup>d</sup> Blackland Research and Extension Center, 720 E. Blackland Road, Texas A&M University System, Temple, TX 76502, USA

### ARTICLE INFO

#### Article history:

Received 22 November 2008

Received in revised form 18 June 2009

Accepted 24 June 2009

Available online 18 July 2009

#### Keywords:

Temporal-spatial dynamics

Land cover status

NDVI

Non-point source nutrient pollution

### ABSTRACT

The temporal-spatial interaction of land cover and non-point source (NPS) nutrient pollution were analyzed with the Soil and Water Assessment Tool (SWAT) to simulate the temporal-spatial features of NPS nutrient loading in the upper stream of the Yellow River catchment. The corresponding land cover data variance was expressed by the normalized difference vegetation index (NDVI) that was calculated from MODIS images. It was noted that the temporal variation of land cover NDVI was significantly correlated with NPS nutrient loading. The regression analysis indicated that vegetation not only detained NPS nutrient pollution transportation, but also contributed to sustainable loading. The temporal analysis also confirmed that regional NDVI was an effective index for monthly assessment of NPS nitrogen and phosphorus loading. The spatial variations of NPS nutrient loading can be classified with land cover status. The high loadings of NPS nitrogen in high NDVI subbasins indicated that forestry and farmland are the main critical loss areas. Farmland contributed sustainable soluble N, but the loading of soluble and organic N from grassland subbasins was much lower. Most P loading came from the areas covered with dense grassland and forestry, which cannot directly discharge to local water bodies. However, some NPS phosphorus from suburban farmland can directly discharge into adjacent water bodies. The interactions among nutrient loading, NDVI, and slope were also analyzed. This study confirmed that the integration of NPS modeling, geographic information systems, and remote sensing is needed to understand the interactive dynamics of NPS nutrient loading. Understanding the temporal-spatial variation of NPS nutrients and their correlations with land cover will help NPS pollution prevention and water quality management efforts. Therefore, the proposed method for evaluating NPS nutrient loading by land cover NDVI can be an effective tool for pollution evaluation and watersheds planning.

© 2009 Elsevier B.V. All rights reserved.

### 1. Introduction

The watershed-land cover variation and its impact on non-point source (NPS) nutrient pollution can lead to serious water quality concerns (George et al., 2008; Chang, 2008). The NPS nutrient pollutants, such as nitrogen (N) and phosphorus (P), are significantly related to land cover status and are direct cause of eutrophication (Ahearn et al., 2005; Azzellino et al., 2006). Traditional monitoring cannot provide the necessary information for the environmental management of a river watershed. Furthermore, the NPS pollution simulation does not provide an effective description of land cover variation because it includes the impacts of temporal varia-

tion of land cover and is in need of diverse spatial and input data (Haregeweyn and Yohannes, 2003). The integration of the NPS simulation model and geographic information system (GIS) can resolve these problems in river basin water quality management, and this combined system is an effective method for identifying the influence of land cover variation as at temporal-spatial scale (Ning et al., 2006). This paper is a pilot attempt to discover the temporal and spatial correlation between land cover and NPS nutrient pollution with GIS and a simulation model at the watershed scale and to explore the role of land cover zoning with different normalized difference vegetation indices (NDVI) in dynamic NPS nutrient settings.

Several methods have been proposed for simulating nutrient loads in a water body, which is a great need in water pollution prevention and source identification (Xian et al., 2007). Most of the model systems can simulate the yield of total nitrogen and phosphorus based on the summation of modeling cells and discharge rate (Yuan et al., 2007; Gowda et al., 2008). However, the variation

\* Corresponding author at: School of Environment, State Key Laboratory of Water Environment Simulation, Beijing Normal University, Beijing 100875, China.  
E-mail address: [wei@itc.nl](mailto:wei@itc.nl) (W. Ouyang).

of land cover at the temporal-spatial scale cannot be considered. On the other hand, the loading differences of diverse land cover categories were measured in small areas, which cannot be applied in water quality control. Based on remote sensing data, the spatial relationship of land cover variation and the variance of nutrient yield has attracted some attention (Krause et al., 2008). In addition to the influence of land cover, precipitation is another significant factor for NPS nutrient yield. The normalized difference vegetation index was applied to express the land cover status, which is directly linked to precipitation (Brunsell, 2006).

In the past, regional land covers were investigated by remote sensing LANDSAT Multispectral Scanner (MSS) and Thematic Mapper (TM) data (Oki and Yasuoka, 2008). In order to get consistent data from images in temporal scale, coarse resolution images were widely used. The NOAA Advanced Very High Resolution Radiometer (AVHRR) image was used to describe land cover transformations at a global or watershed scale (Vicente et al., 2006). In this study, land cover NDVI information was calculated with imagery from Moderate Resolution Imaging Spectroradiometer (MODIS). The MODIS instrument on board NASA's Terra satellite is designed primarily for remote sensing the land surface with spatial resolutions of 250 m (Stefanov and Netzbund, 2005). Moreover, frequent temporal resolution can provide fine repeated data, providing a good method for monitoring and analyzing vegetation processes. MODIS has been popularly applied in a variety of projects involving large scale vegetation dynamics and land coverage research (Wardlow and Egbert, 2008).

Most of the NPS modeling systems have the ability to estimate the discharge of annual nitrogen and phosphorus loads (Flipo et al., 2007). However, the discharge sum of basin calculation cells can only evaluate the load of each watershed. In other words, it is not easy to simulate the temporal-spatial characteristics of NPS nutrient load, which is the basis for land cover variation correlation identification in watersheds. To achieve these results, the Soil Water Assessment Tool (SWAT) was applied to simulate temporal-spatial variations in NPS nitrogen and phosphorus discharge from the defined watershed (Chaplot, 2005). The SWAT model makes more sustainable progress than the conventional empirical models and can export the loadings in different forms of nutrient pollution (Behera and Panda, 2006).

SWAT is a watershed NPS pollution modeling system developed by the United States Department of Agriculture-Agriculture Research Service (USDA-ARS). SWAT was used in this study for its ability to simulate watershed NPS pollution processes at basin and subbasin scales (Abbaspour et al., 2007). The subbasin application is beneficial for estimation processes, especially when dealing with different types of land cover and soil types distributed throughout the simulated watershed (Arnold et al., 2000). Also, the subbasin is further delineated into hydrologic response units (HRUs) for the soil-land use threshold percentage. In regard to the temporal scale, the SWAT model is a physically based simulation method that can run at a continuous, daily time-step (Arnold et al., 1998). The temporal and spatial resolution of nutrient pollution simulated by SWAT is the critical basis for the following analysis in this paper.

In this study, nutrient yields were mapped in different forms throughout the whole basin and every subbasin using the SWAT model. The monthly and yearly loading of each form of NPS nutrient were estimated, respectively. Therefore, 16-day maximum NDVI data calculated from MODIS imagery with spatial resolutions of 250 m was used to observe land cover dynamics in yearly and monthly temporal scale as well as basin and subbasin spatial scale. The relationship between land cover dynamics, estimated from monthly NDVI images, was compared with the monthly yield of NPS nitrogen and phosphorus. Furthermore, the spatial correlation of NPS nutrient pollution and land cover at the subbasin scale

was summarized, which lead to the conclusion about the potential impact of land cover on NPS pollution.

## 2. Materials and methods

### 2.1. Description of example study area

The study area includes the main catchments of the upper stream of the Yellow River and is the connection of the Qinghai-Tibet Plateau and the Loess Plateau (Fig. 1). The climate in this area is typical of the continental region—cold, dry and with obvious seasonal variation. The average annual precipitation is about 411 mm, mainly falling as snow or storm runoff, and the average yearly temperature is about  $-2.3^{\circ}\text{C}$ , without an absolutely frost-free season (Feng et al., 2005). Grassland is the principal land cover in this watershed. The village and farmland are concentrated along the main stream and reservoirs. Diverse vegetation is distributed in different elevation areas. The cold steppe appears in the area with elevation between approximately 3000 and 4100 m. In the lower elevation area between 2500 and 3300 m, the land is covered mainly by shrub-arbor. The temperate shrub-meadow steppe only appears in the area of elevation between 2200 and 2800 m. Some desert steppe spreads between the elevation of 1700 and 2200 m (Wang et al., 2000; Wu, 2004). In recent decades, desertification is the main environmental degradation concern in this region and imposes a great threat to regional environmental stability (Wang et al., 2006).

### 2.2. General research framework

The general framework of the present study is illustrated in Fig. 2. First, the SWAT-required spatial database was constructed then the model system was calibrated. Secondly, monthly and yearly NPS nutrient yields, in their different forms, were estimated at basin and subbasin scales. Thirdly, the land cover dynamics in the same temporal-spatial scale were calculated with MODIS images using ArcGIS. With statistical analyses, the temporal correlations of land cover NDVI with NPS nutrient loadings from the whole basin were identified. Furthermore, the spatial interaction of land cover at the subbasin level was calculated with corresponding NPS nutrient discharge.

### 2.3. Theory description of SWAT

Using input databases, SWAT simulates hydrology, soil erosion, and nutrient loading. Hydrological process modeling is the first step for nutrient pollution modeling and follows the water balance equation, consisting of four parts (i.e. surface runoff, evapotranspiration, soil water, and groundwater). Soil erosion is simulated with the Modified Universal Soil Loss Equation (MUSLE), which takes into consideration factors such as runoff, peak runoff rate, soil erodibility, soil management, support practices, topography and coarse fragments (Williams, 1995). During nitrogen cycle simulation, SWAT identifies the transformation of five forms of nitrogen and estimates their yield, respectively. In this paper, the nitrogen is separated into two groups, soluble and organic. Soluble N is the inorganic form of nitrogen,  $\text{NH}_4^+$  and  $\text{NO}_3^-$ . Organic N relates mainly to soil humus, crop residue, and microbial biomass. In regard to phosphorus cycle simulation, the model can estimate six forms and categorize them into organic P and sediment P. The organic P, including fresh, active, and stable organic P, comes from crop residue, soil humus, and microbial biomass. The sediment P is the amount of P discharged into water with the sediment. In consideration of correlation analysis and application in regional environmental management, the temporal-spatial variations of total nitrogen (TN) and total phosphorus (TP) were also calculated (Arnold et al., 1998).

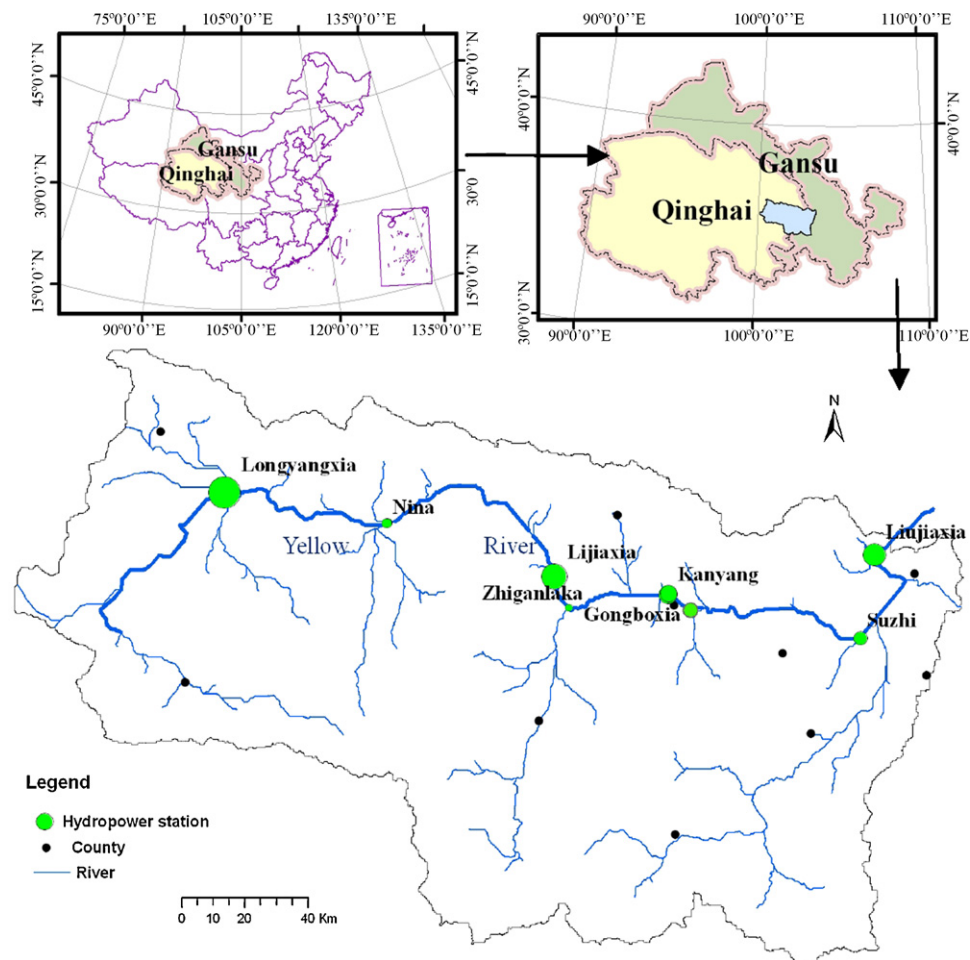


Fig. 1. Study area location in the upper stream of Yellow River.

#### 2.4. Model inputs

The necessary input databases for SWAT simulation are prepared (Table 1). The spatial databases regarding topography, land use, and soil properties were developed and reclassified by the model. The watershed management information was applied to improve modeling accuracy. The characteristics of the watershed climate were simulated with daily, historical monitoring data from 1990 through 2006, collected from six weather stations around study area (Fig. 4).

Fig. 3 shows the observed land use distribution of the watershed in 2000. There is more vegetation cover in the eastern and southern areas than in the western and northern areas. Most barren lands appear in the western area, while forests and dense grassland are widespread in the southern basin. The agricultural land is close to water and centers around the reservoir in the eastern portion and along the main stream of the Yellow River. Grassland is the principal land cover and constitutes about 62.01% of the study area. Forests and farmland cover 14.29% and 11.46%, respectively.

Soil property is another key factor for nutrient formation and loading, although it did not change for several decades. There are thirteen categories of soil in this research basin (Fig. 4). The soil property indices including area, percentage, coarse sand, fine sand, silt, clay, organic carbon, TN, TP and total potassium are listed in Table 4. The dominant soil types in this area are *Chestnut soil* and *Meadow chernozem*. The *Chestnut soil* occupies nearly half of the area and its TN, TP content is 0.18% and 0.08% respectively. The *Meadow chernozem* dominates another 23.55% of the area and has a higher content of TN (0.25%). The *Grey desert soil* spreads along the main stream of the Yellow River, which has direct impact on water quality. The TN and TP contents of this soil are 0.07% and 0.10% respectively.

#### 2.5. Model calibration

Expert advice and historical water quality and stream flow monitoring data were used to calibrate the AVSWAT model (Table 2) (Ouyang et al., 2008a,b). Only limited observed flow and sediment data were available for this study. First sensitivity analysis

**Table 1**  
Data type scale and data description.

Data type	Scale	Data description
Topography	1:250,000	Elevation, overland and channel slopes and lengths
Land use	1:1,000,000	Land use classifications
Soil properties	1:1,000,000	Soil physical and chemical properties
Weather	6 stations	Daily precipitation, wind, solar radiation, and temperature
Land management information	–	Fertilizer application, planting, and harvesting

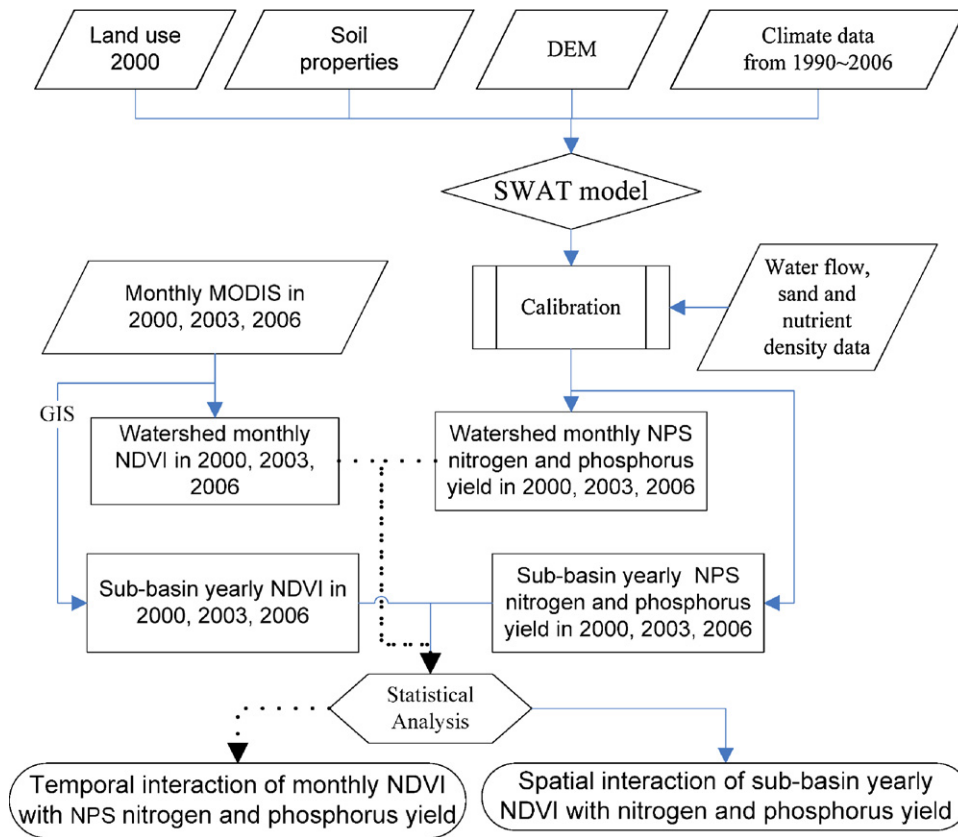


Fig. 2. The general framework of this paper.

was performed for the study watershed and only most sensitive parameters were selected to perform additional manual calibration. The process lasted from January 2000 to December 2002. Six stream flow related parameters were adjusted to correct for water flow overestimation. The sand density and water flow data at the outlet of the study area were used to calibrate six more soil erosion related parameters. Considering that there were three main land covers, *canmx* and  $C_{USLE}$  indices were used for

the three leading vegetations leading to more accurate modeling result.

Fig. 5A shows a comparison between the observed and simulated monthly water flow. The coefficient of correlation (0.7261) indicates that the simulated data is close to the observed value. In general, the intersection (0.7472) shows that the simulated water flow was under simulated as compared to the observed data. Fig. 5B demonstrates the difference between the simulated and observed

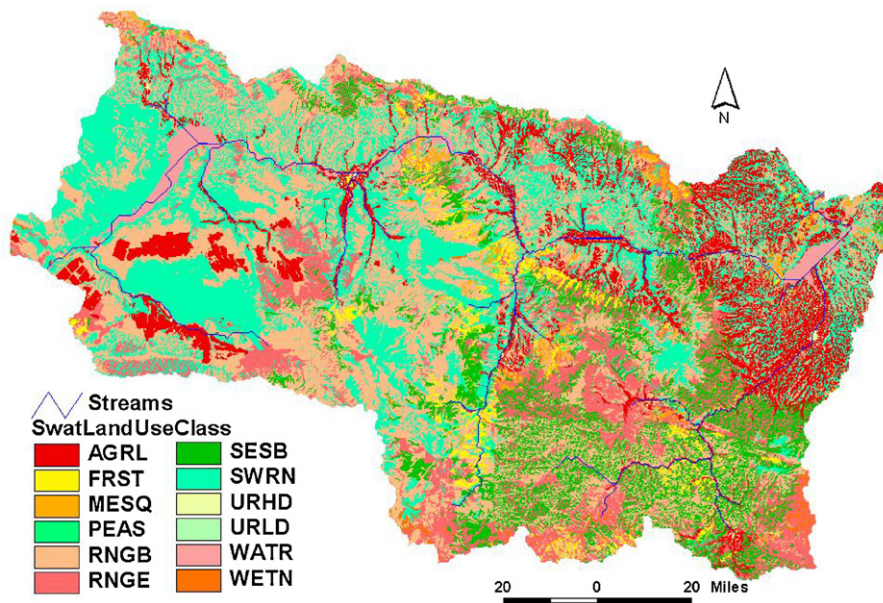


Fig. 3. Land cover distribution in study area.

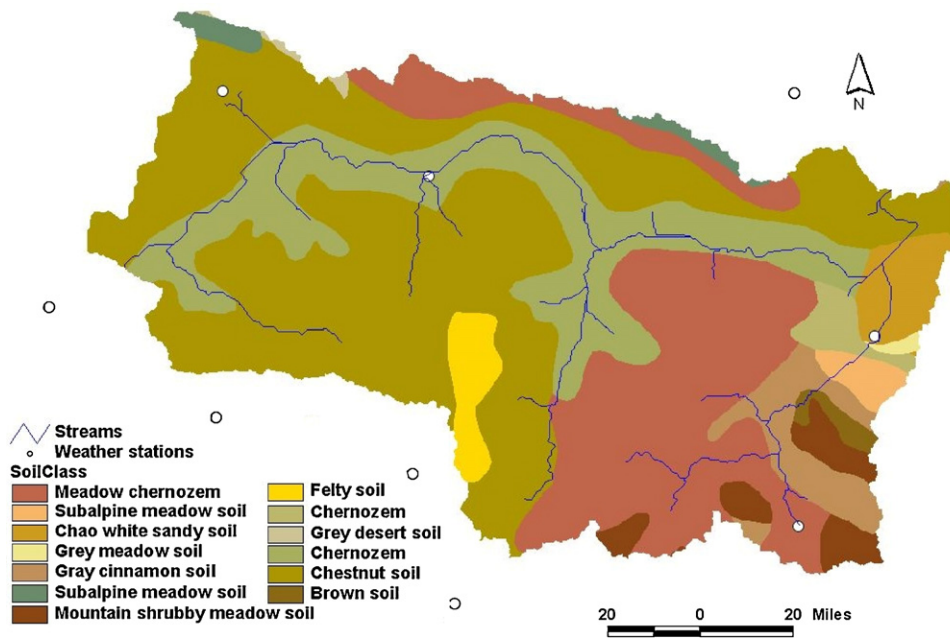


Fig. 4. Distribution of watershed soil types and weather stations.

monthly soil erosion. The improved coefficient of correlation indicates the soil erosion simulation is more accurate than the water flow. However, the lower intersection means that the simulated soil erosion load was still underestimated. This may be due to the under prediction of water flow. Given the limited amount of observed data, the simulation of water flow and soil erosion is reasonable.

After validating the water flow and soil erosion, the next step was to calibrate nutrient parameters, which was difficult for lack of monitoring data. Seven principle N and P discharge parameters are listed in Table 2 after sensitive analysis. However, there was no regular organic or inorganic N or P monitoring in this area. Consequently, the TN monitoring data were applied in N calibration (Misgana and John, 2005). With TN monitoring data from Zhang et al. (2003), the monthly TN yield was validated first. The comparison of simulated and recorded TN is given in Fig. 6A. It was also noted that there is a ratio between NPS nitrogen and phosphorus yield in a predefined basin (Ouyang et al., 2008a,b). In the Yellow River watershed, Yang et al. (2006) has calculated the yield ratio of TP and TN resulting in a value of 0.1304. The P simulation parameters were validated with this ratio. The monthly yield ratio ranged

from 0.16 and 0.08 and the average ratio was 0.12 (Fig. 6B). Based on the limited data and acceptable results, the model system was validated and ready for simulation.

2.6. NDVI data procedure

The land cover NDVI data were extracted from MODIS images (MOD13Q1, h26 v05), which downloaded from the Land Processes Distributed Active Archive Center at NASA. The NDVI values were calculated with reflectance of red band (610–680 nm) and near infrared band (780–890 nm), which have been corrected for molecular scattering, ozone absorption, and aerosols. The 250 m spatial resolution NDVI images were repeated over a cycle of 16 days (Pontus et al., 2007). According to local land cover and climatic characteristics, a monthly series of MODIS images were taken from February 18 to December 18 in 2000, 2003 and 2006 and were implemented to express land cover variation. The original MODIS images were mosaic and georeferenced to the Universal Transverse Mercator (UTM) projection system by the nearest-neighbor resampling method (William and Maik, 2005). With ArcGIS 9.2,

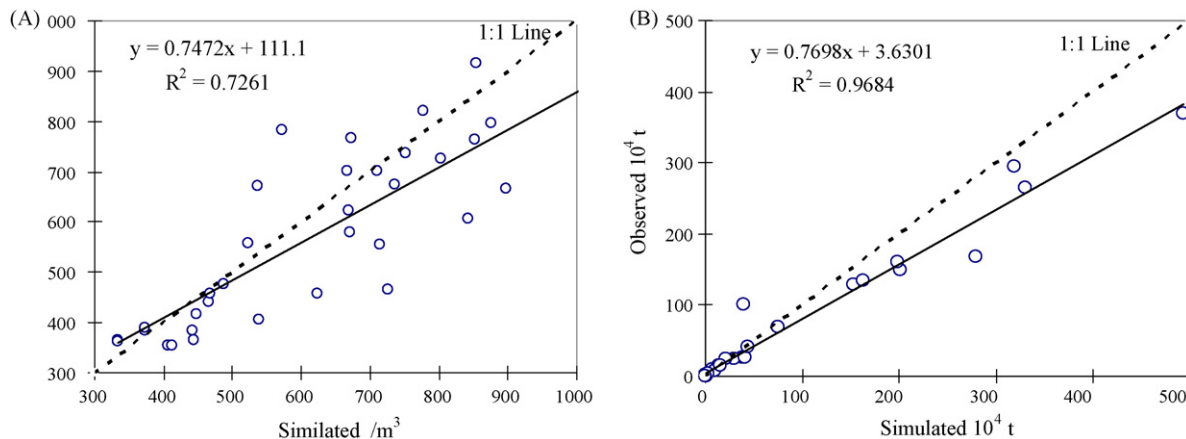


Fig. 5. Comparison of simulated and observed monthly water flow and soil erosion from 2000 to 2002.

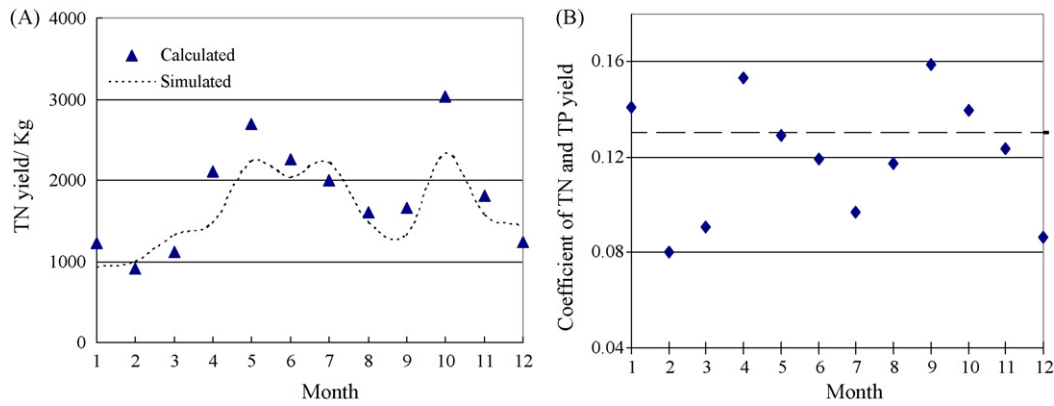


Fig. 6. Comparison of simulated and calculated monthly total nitrogen and total phosphorus yield.

Table 2  
SWAT model parameters for model calibration.

Parameter description	Calibration value
Curve number ( $CN_2$ )	61
Plant water uptake compensation factor ( $SOL\_AWC$ )	0.04
Soil evaporation compensation factor ( $ESCO$ )	0.41
Groundwater delay coefficient ( $GW\_DELAY$ )	30.1
Amount of shallow aquifer water that moved into the soil profile ( $GW\_REVAP$ )	0.1
Maximum canopy storage ( $canmx$ )	Grassland: 3.5 Farmland: 2.2 Forestry: 4.2
Threshold depth of water in shallow aquifer for "revap" or percolation to deep aquifer ( $REVAPMN$ )	200
Base flow alpha factor ( $ALPHA\_BF$ )	0.03
Average slope steepness ( $SLOPE$ )	0.129
Average slope length ( $SLSUBBSN$ )	26.15
Maximum amount of sediment ( $SPCON$ )	0.001
Sediment restrained in channel ( $SPEXP$ )	1.21
Universal Soil Loss Equation factor ( $C_{USLE}$ )	Farmland: 0.25 Forestry: 0.10
Initial humic organic N in soil layer ( $SOL\_ORGN$ )	5000
Initial humic organic P in soil layer ( $SOL\_ORGP$ )	1500
Initial $NO_3$ concentration in soil layer ( $SOL\_NO_3$ )	3500
Nitrate percolation coefficient ( $NPERCO$ )	0.25
P percolation coefficient ( $PPERCO$ )	12.5
P soil partitioning coefficient ( $PHOSKD$ )	160
Biological mixing efficiency ( $BIOMIX$ )	0.25

the basin and subbasin NDVI tempo-spatial variation characteristics were calculated and demonstrated. The monthly NDVI was the average value of the whole watershed. The yearly NDVI of every subbasin was calculated using following procedure: (1) the 12 monthly images of basin NDVI were summed and averaged; (2) the average subbasin value was extracted using the zonal statistics tool.

### 3. Results

#### 3.1. Temporal-spatial trends of the NDVI

##### 3.1.1. Spatial trends of the NDVI

With MODIS images, the yearly NDVI distributions in 2000, 2003, and 2006 are shown in Fig. 7. Comparing the three years, the NDVI distribution did not experience substantial variation. The western portion and areas along the river bank distinguished the

lower NDVI from the area of higher NDVI which was spread mainly throughout the south-eastern region. The NDVI ranges during the three years were 0.9173, 0.9233, and 0.8921, respectively. In 2003, the largest NDVI range was impacted directly by a greater amount of precipitation. The spatial variation of NDVI was created by extracting the NDVI value in every subbasin cell, assisted by the ArcGIS tool. At the subbasin level, the NDVI range in 2000, 2003, and 2006 were 0.5347, 0.4690, and 0.5159, respectively. The NDVI in 2003 had the smallest range and standard deviation, which indicated that the subbasin NDVI was more similar than in the other years. With the subbasin mean NDVI data, the vegetation status in each cell can be expressed, which was the basis for interaction analysis.

##### 3.1.2. Temporal trends in basin NDVI

The monthly NDVI data were averaged with MODIS data by ArcGIS (Table 3), which presented the temporal variation principle of watershed land cover. The monthly pattern showed similar trends during the three years, describing vegetation growth dynamics. The NDVI increased dramatically from April and reached its summit in July, then decreased slowly throughout the remainder of the year. Overall, the NDVI range during the three-year period dropped from 0.3669 to 0.3017, which also caused the standard deviation (Std. D.) to continually decrease from 0.1342 to 0.1245. However, the mean NDVI value increased from 0.2885 to 0.3172 in the same period. The minimum NDVI in 2000 was 0.1228, which was significantly less than the other two years. The lower NDVI value in 2000 was consistent with the drought in that year. The NDVI

Table 3  
Watershed monthly NDVI value and statistical feature.

Month	Year		
	2000	2003	2006
1	0.1228	0.2076	0.1904
2	0.1305	0.1948	0.1874
3	0.1884	0.1868	0.1943
4	0.2062	0.2143	0.2441
5	0.3945	0.3912	0.4186
6	0.4897	0.4507	0.4874
7	0.4579	0.5178	0.4891
8	0.4453	0.5028	0.4684
9	0.3661	0.3708	0.3927
10	0.2642	0.2741	0.2799
11	0.2195	0.2350	0.2568
12	0.1767	0.1584	0.1963
Range	0.3669	0.3594	0.3017
Mean	0.2885	0.3087	0.3171
Std. D.	0.1342	0.1309	0.1245

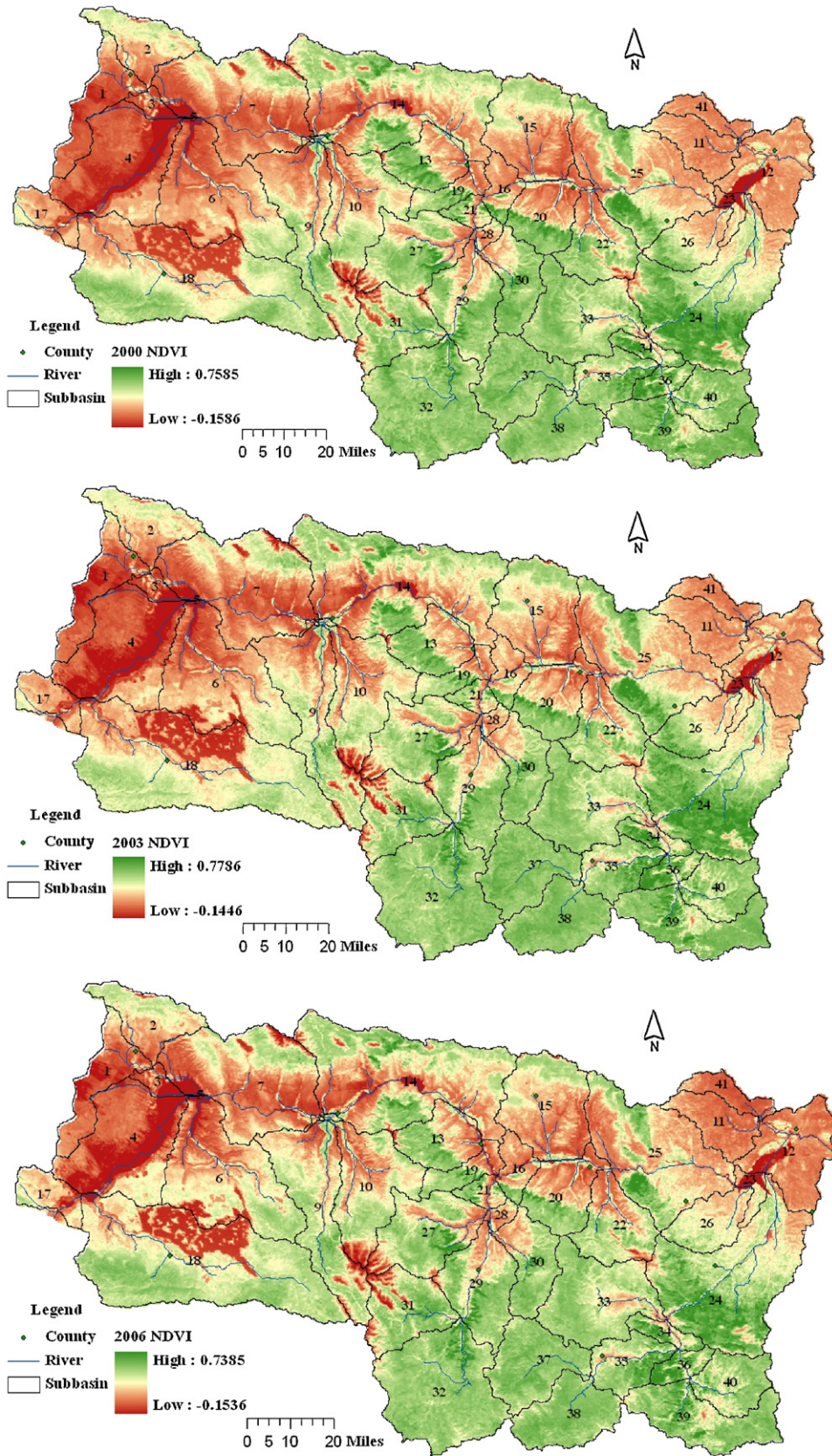


Fig. 7. NDVI distribution of each subbasin in three years.

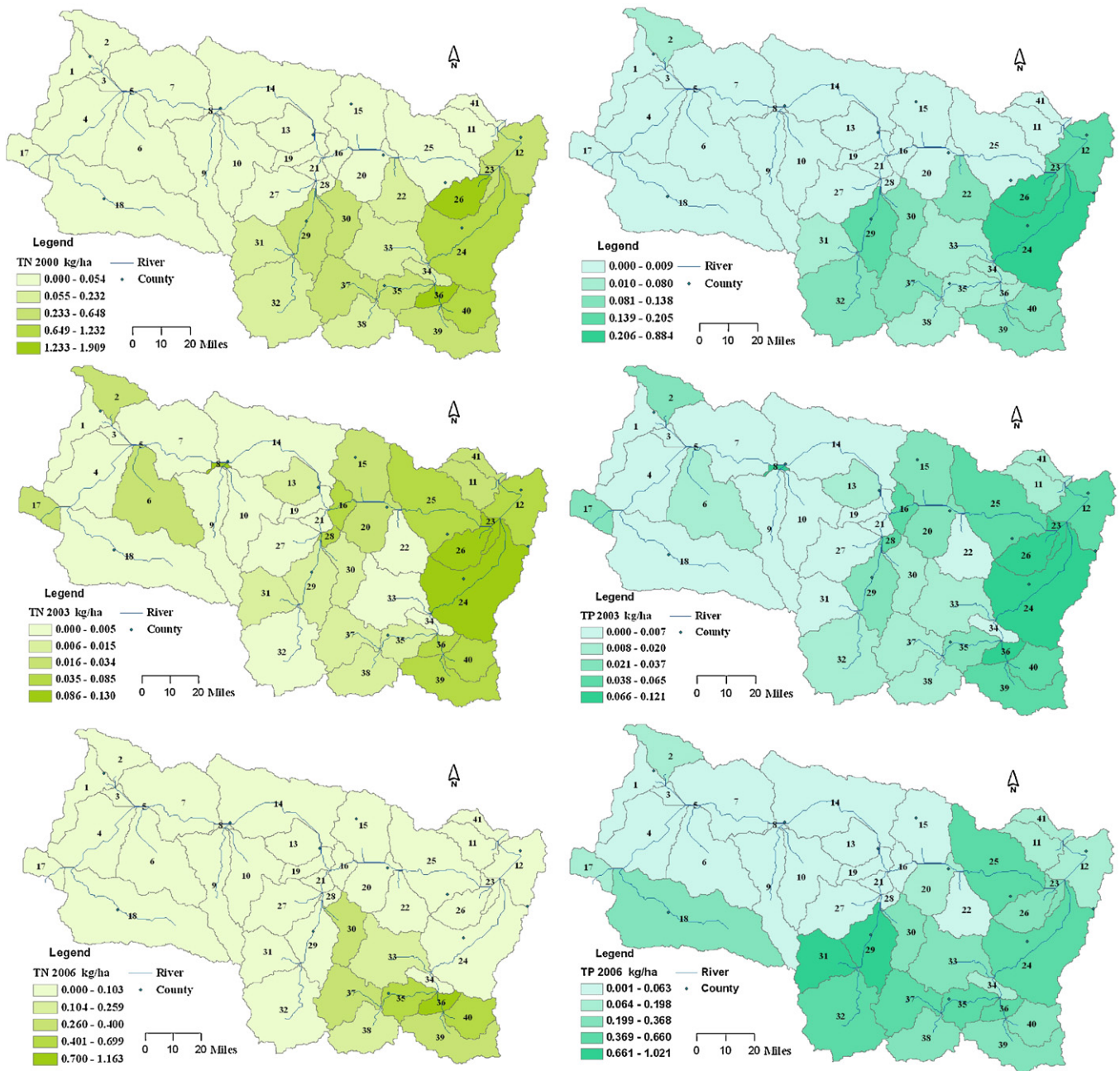


Fig. 8. TN and TP loading distributions for each subbasin during the three years.

demonstrated the features of land cover and precipitation, which are the dominant factors for soil erosion formation and transportation.

### 3.2. Spatial trends of NPS nitrogen pollution

#### 3.2.1. Spatial trends of NPS nitrogen loss

The annual load of TN and TP during the three simulated years is shown in Fig. 8. NPS nitrogen loadings from different subbasins showed significant spatial differences, showing an increasing trend from west to east in the observed watershed. In the northeast region, TP loadings ranged from 0.005 to 1.718 kg/ha. The critical loading subbasins were distributed in the east, while the farmlands were distributed predominantly around the Liujiaxia reservoir and along the main stream of the Yellow River. The spatial distribu-

tion observed throughout the three years contained similar trends, and the subbasins covered with more vegetation had a remarkable association with TN loading.

#### 3.2.2. Temporal trends of NPS nitrogen

The monthly TN loading for the three years is listed in Table 4. The monthly load had a significant temporal trend. The TN loading increased from January to July then declined, which paralleled the similar temporal pattern of vegetation growth. The maximum loadings were recorded in June and July as 0.105, 0.753 and 0.096 kg/ha in 2000, 2003, and 2006, respectively. The annual loading of NPS nitrogen in 2003 was much more than the other two years. This may be due to the combined effects of land use variation and storm rain. Although there were some variances in monthly loading, the temporal pattern was constant.

**Table 4**  
Watershed monthly TN load (kg/ha) and statistical feature.

Month	Year		
	2000	2003	2006
1	0.000	0.000	0.000
2	0.002	0.003	0.000
3	0.004	0.037	0.000
4	0.000	0.106	0.002
5	0.020	0.074	0.002
6	0.060	0.007	0.096
7	0.105	0.753	0.081
8	0.010	0.342	0.047
9	0.037	0.189	0.038
10	0.010	0.354	0.010
11	0.002	0.044	0.008
12	0.003	0.001	0.005
Range	0.105	0.753	0.096
Mean	0.021	0.159	0.024
Std. D.	0.032	0.226	0.034

3.3. Spatial trends of NPS phosphorus pollution

3.3.1. Spatial trends of NPS phosphorus loss

The watershed TP loadings in 2000, 2003, and 2006 were simulated and the annual distributions were shown in Fig. 8. NPS phosphorus yields from individual subbasins had a high spatial variability, but the spatial distribution during the three years followed similar trends. Approximately half of the basin contributed very little P (0.008 kg/ha) and did not critically impact water quality. However, some subbasins in the eastern and southern areas contributed much more TP, which had loadings in excess of 0.1 kg/ha. The No. 29 subbasin in the middle reach had the most remarkable loss. The spatial distribution coincided with vegetation trends, indicating that vegetation, especially forest and dense grass, has a direct relationship with NPS phosphorus pollution. The spatial distribution of NPS phosphorus was also useful for identifying the transportation path.

3.3.2. Temporal trends of NPS phosphorus

The estimated monthly TP load during the three years shared similar temporal patterns with TN. The TP loading exhibited an upward trend from January to August then decreased. The highest yearly and monthly loads were both in 2006. The peak value of monthly loading in these years appeared in June and July, which coincided with summit TN loadings. The maximum loads throughout the three years were 0.048, 0.042, and 0.088 kg/ha, respectively, causing corresponding variation in the standard deviation (Table 5).

**Table 5**  
Watershed monthly TP load (kg/ha) and statistical feature.

Month	Year		
	2000	2003	2006
1	0	0	0
2	0.002	0	0
3	0.004	0.004	0
4	0	0.005	0.08
5	0.021	0.007	0.002
6	0.048	0.002	0.002
7	0.002	0.042	0.088
8	0.007	0.026	0.046
9	0.012	0.011	0.036
10	0.004	0.019	0.01
11	0	0	0.007
12	0.002	0	0.004
Range	0.048	0.042	0.088
Mean	0.009	0.010	0.023
Std. D.	0.0139	0.0131	0.0322

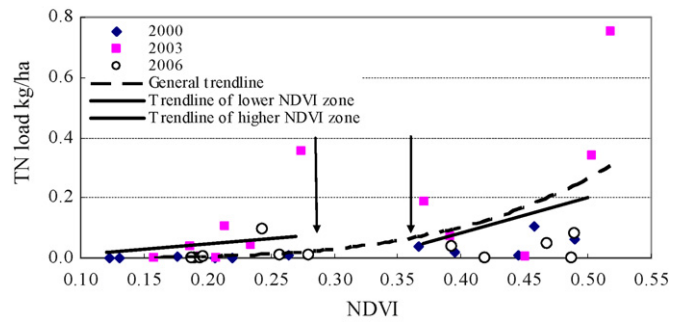


Fig. 9. Temporal interaction between watershed NDVI and monthly TN loss.

4. Discussion

4.1. Influence of NDVI temporal variation on NPS nutrient loads

4.1.1. NPS nitrogen

The monthly basin NDVI can be used as an indicator for NPS nitrogen loading, as the correlation between them shows (Fig. 9). It was concluded that the variation of TN loss had considerable connection with the temporal scale of watershed land cover. When watershed NDVI was less than 0.27, the NPS total nitrogen loading was much lower. Local vegetation NDVI increased quickly in the summer, so there was an NDVI gap during correlation analysis. However, the TN loss increased dramatically when land cover had an NDVI higher than 0.35. Previous studies have concluded that more vegetation can prevent NPS pollution (Maillard and Santos, 2008). The analysis indicated that vegetation not only disturbed pollutant transportation, but contributed sustainable NPS pollution. During the period of vegetation growth and maturity, the increasing NDVI and its associated precipitation intensified NPS loadings. This delivery certainly impacted the water quality and terrestrial ecosystem. The regression analysis indicated that the monthly NDVI was a good predictor for determining monthly NPS total nitrogen pollution load.

4.1.2. NPS phosphorus

The temporal correlation pattern between the monthly variation in land cover on the formation and transportation of TP loadings was confirmed (Fig. 10). When the average watershed NDVI was lower than 0.28, much less NPS phosphorus pollution occurred. Watershed TP yields increased when the NDVI value was higher than 0.35. There was an obvious threshold point in TP loading at which watershed NDVI jumped from 0.28 to 0.35. In preventing NPS phosphorus pollution, the critical time period is the moment of higher NDVI. Human engineering solution should be applied during the time of higher NDVI, resulting in better water quality. The regression analysis also confirmed that regional NDVI was an

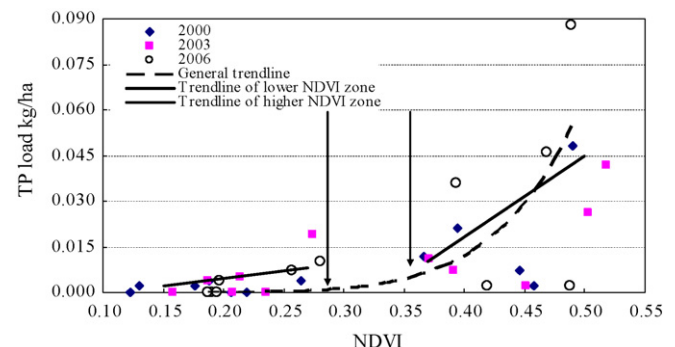


Fig. 10. Temporal interaction of watershed NDVI with monthly TP loss.

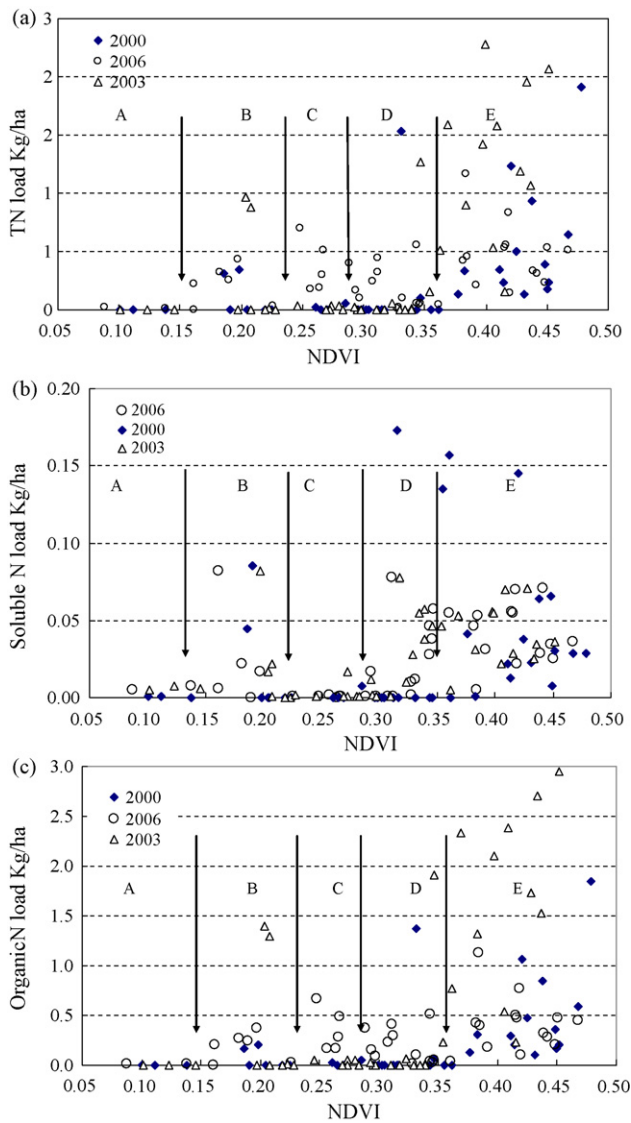


Fig. 11. Interaction of annual subbasin NDVI with N loss.

effective index for monthly assessments of NPS total phosphorus discharges.

#### 4.2. Subbasin NDVI with NPS nitrogen pollution

In order to recognize the influence of land cover status on NPS nitrogen loading, the correlation between NDVI and TN, organic N, and soluble N was calculated at the subbasin level (Fig. 11). It was found that subbasin NDVI was a significant factor in NPS nitrogen yield. The subbasins with an NDVI lower than 0.15 contributed almost no NPS nitrogen, differing from areas with high soil erosion. Preventing NPS nitrogen discharges from areas with dense vegetation was the highest priority for pollution control. Furthermore, forest and dense grass were found to have more influence on NPS nitrogen loading than other land covers. After classifying the land covers by NDVI, the gathering plots were defined in five zones. In forested subbasins (zone E), the NPS nitrogen load was much higher than other zones. The NPS nitrogen load discharged from bare land and grassland areas (zone A and zone C) was much lower. The cultivated subbasins (zone B) contributed some NPS nitrogen. Based on an NDVI value from a predefined subbasin, the NPS total nitrogen load from each subbasin can be estimated, which was helpful for a quick assessment of pollution loads.

Furthermore, the correlation of land cover NDVI with soluble N and organic N were analyzed. Soluble N loading was a small portion of TN loss, but it had a more significant link with subbasin NDVI. As seen in Fig. 11b, the soluble N discharge was higher in zone B than organic N. The higher load in zone B was due to the loss of fertilizers. Soluble N discharged from forested areas was due to arboreal remains. However, the soluble N yield from subbasins covered with dense grass was very low due to the uptake by grass. The findings in this study confirm that grassland strips are an effective way to prevent NPS soluble N from discharging into the aquatic environment. Fig. 11c shows the relationship between organic N loading and NDVI. Unlike the remarkable load of soluble N in zone B, the organic N yield from this zone was relatively slight. On the other hand, the organic N discharge value was the same for both the grass and forested subbasins. This was due to the fact that most organic N was transported with the soil particle. The subbasin characterized with dense grass was still the key for organic N.

Overall more loading of NPS nitrogen in higher NDVI subbasins indicated that forests and farmland were the critical loss sources. The key to preventing NPS nitrogen is to disturb the transportation paths, as demonstrated by the fact that the loading of soluble and organic N in the grassland subbasins was much lower. In addition, other studies have shown that grassland can reduce particle movement and is more effective in detaining N (Merrill and Benning, 2006). Based on the findings of this study and the conclusion of the aforementioned study, setting aside grassland strips along the critical subbasin is probably the most effective solution to reducing NPS nitrogen.

#### 4.3. Subbasin NDVI with NPS phosphorus pollution

Following the same procedure, the impact of land cover NDVI on NPS phosphorus loss was analyzed (Fig. 12). The hypothesized NPS phosphorus load differences among the subbasins were confirmed consistently. The first notable trend was that the loading of NPS phosphorus increased with increasing NDVI. As shown in Fig. 12a, forested areas with higher NDVI in zone E contributed sustainable TP yield. The bare land with NDVI less than 0.15 produced almost no NPS phosphorus pollution. The agricultural land with NDVI between 0.15 and 0.23 had a positive association with P loading. The grassland with NDVI between 0.23 and 0.30 was the primary land cover that contributed much less TP loss. On the other hand, grassland has been proven as an effective buffer zone to prevent NPS phosphorus pollution (Bouldin et al., 2004). These results suggested land cover with higher NDVI was the principal driving force for NPS phosphorus pollution.

The relationship between subbasin NDVI and organic and sediment P loadings was further analyzed (Fig. 12b and c). Both forms of P loadings had close linkages with forested areas. The spatial variation of organic P loading was accompanied by NDVI. As shown in Fig. 12b, there was urban sprawl moving into forested areas (zone E) and notable loading decreases from agricultural land (zone B) and dense grassland (zone D). This illustrates that forested areas increase NPS organic P pollution. Runoff from these densely covered subbasins typically contained a high density of NPS phosphorus.

The correlation of NDVI with sediment P is shown in Fig. 12c. There were significant increases in sediment P yield in most subbasins with an NDVI between 0.15 and 0.23 (zone B). This illustrated that agricultural cultivation had a major impact on NPS sediment P pollution. The surplus of P fertilizer and deposition of waste intensified sediment P loss. Unlike the scenario with organic P, the subbasins covered with dense grassland (zone D) had higher loading. Equally, the forested subbasins contributed significant sediment P loading. There were no significant differences between the yield of organic P and sediment P in zone E, which included higher NDVI subbasins in the mountainous region.

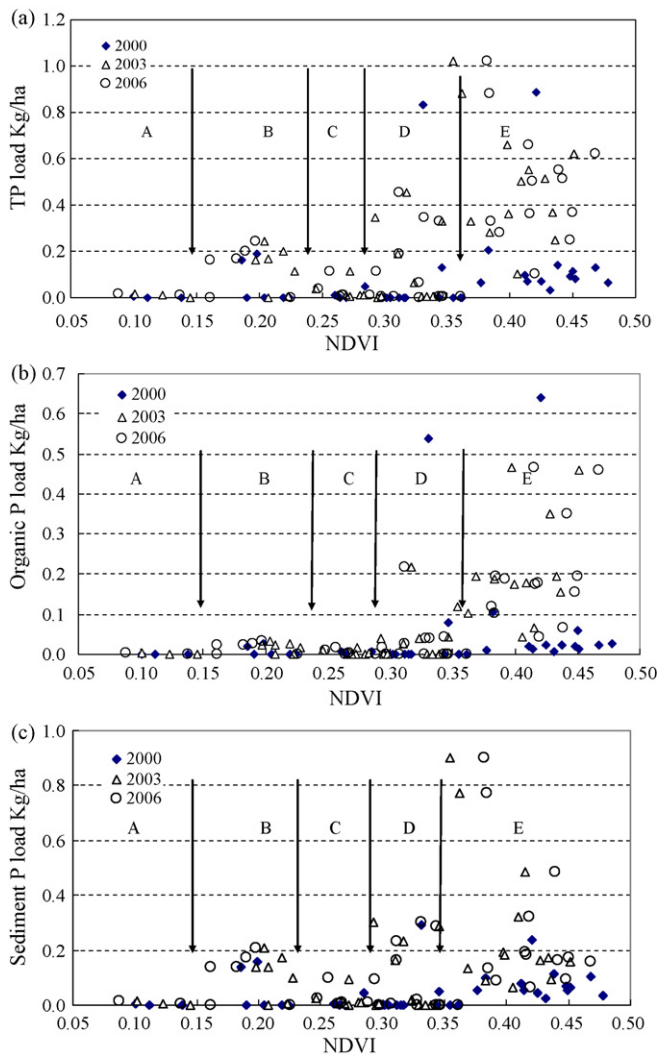


Fig. 12. Interaction of annual subbasin NDVI with P loss.

Except NPS phosphorus from farmland, most P loading came from the area with dense grassland and forests, which cannot directly discharge into local water bodies. Engineering structures should be constructed along the forested subbasins, effectively preventing phosphorus loading. Equally, most NPS phosphorus from suburban farmland discharges directly into adjacent water bodies. In riparian systems, the agricultural P loading can be prevented through best management practices.

#### 4.4. Slope, NDVI and nutrients load

As seen in Figs. 11 and 12, there were some outlying points and clustered points. In order to explain this and the intensified impact of slope, the interrelationship of slope, annual NDVI, and yearly nutrient loads were analyzed (Fig. 13). Slope was a compensatory signal for erosion. Consequently, the analysis demonstrated that the critical TN loss area was the subbasin with higher NDVI. The NDVI status had more direct impact on TN loss than the slope condition. The forested mountain area with the steepest slope was a critical TN discharge source. The forested subbasins with a slope of 6–8° contributed to TN loading. The discharge source of TP was much more complicated. The slope was more sensitive than NDVI in regard to TP loss. Therefore, the critical areas had a slope higher than 10° with an NDVI ranging from 0.32 to 0.47. However, there was another zone that had a remarkable TP yield with an NDVI

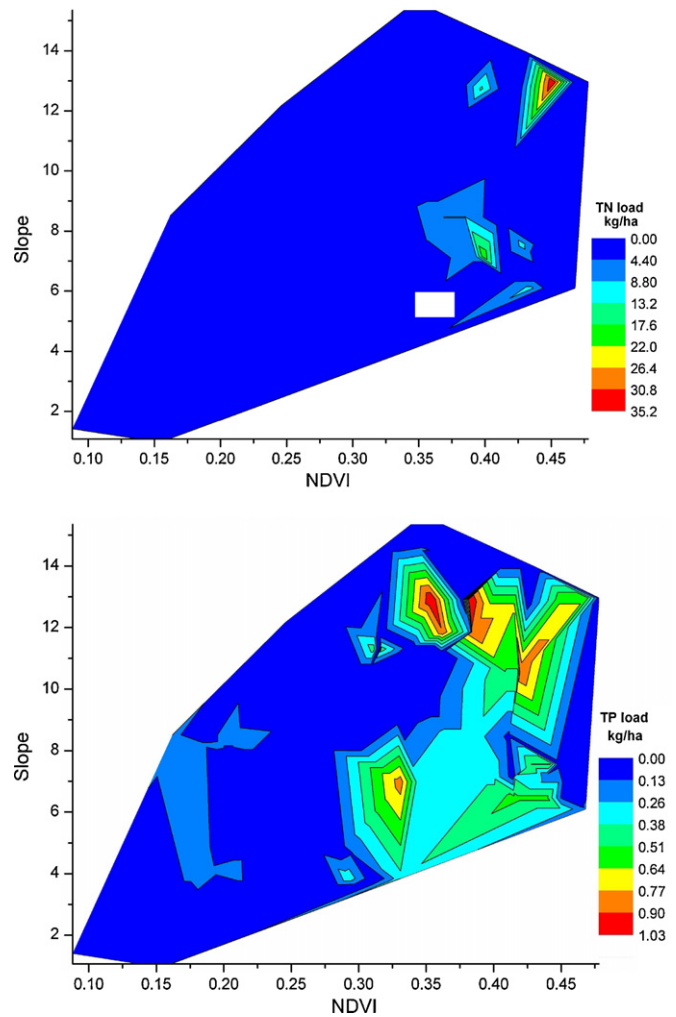


Fig. 13. Interaction of subbasin NDVI and slope with nutrient loads.

around 0.3 and a slope of 6°. The analyses showed that most of the TP originated from steep, forested areas and dense grassland. The well-preserved, natural plantation was the main contributor of TP loading, not the human activity landscape.

## 5. Conclusions

In this study, we estimated the annual and monthly NPS nutrient loads in the upper stream of the Yellow River catchment using SWAT. The variation principle of land cover status was expressed by NDVI, calculated from MODIS imagery. The study demonstrated that temporal variation of land cover NDVI showed significant correlation with NPS nutrient loading. The regression analysis indicated that vegetation not only prevented NPS nutrient pollution transportation, but also contributed sustainable NPS nitrogen and phosphorus pollution. In the period of vegetation growth and maturity, the increasing NDVI and associated precipitation increased NPS nutrient loadings, which certainly impacted the water quality and terrestrial ecosystem once delivered. The temporal analysis confirmed that regional NDVI was an effective index for the monthly assessment of NPS nitrogen and phosphorus loadings.

The spatial variations of NPS nutrient loads were associated with land cover status. Greater loading of NPS nitrogen in higher NDVI subbasins indicated that forest and farmland are critical loading areas. Farmland contributed sustainable soluble N, but the discharge of soluble and organic N in the grassland subbasins was much lower. The spatial analysis demonstrated that most P load-

ings came from the area covered with dense grassland and forests that cannot directly discharge to local water bodies. On the other hand, some NPS phosphorus from suburban farmland can easily discharge into adjacent water bodies. Setting aside riparian habitat along the critical subbasin, adjacent to farmland and forests, will be the most effective solution for reducing NPS nutrients.

The interaction of slope, NDVI, and nutrient loading identified the nutrient discharge source deeply. The analysis demonstrated that the area with steeper slope and higher NDVI contributed most of the nutrient loadings. The remote, natural plantation was the main source of NPS nutrient pollution in the study watershed rather than being human activity oriented.

This study supports the integration of NPS modeling and land cover monitoring by remote sensing to understand the interactive dynamics of NPS nutrient loading. Understanding the temporal-spatial variation of NPS nutrients and their correlation with land cover will help NPS pollution prevention and water quality management efforts. Therefore, the proposed method for evaluating the NPS nutrient loadings by land cover NDVI is a helpful and effective tool for pollution evaluation and watershed planning.

## Acknowledgements

Without courage and comments from Prof. Andrew K. Skidmore at the International Institute for Geo-Information Science and Earth Observation (ITC) and Prof. Jan de Leeuw at the International Livestock Research Institute (ILRI), Nairobi, Kenya, this paper could not be completed. Two anonymous sources also provided helpful advice. The authors wish to thank the Data Center for Resources and Environmental Sciences Chinese Academy of Sciences (RESDC) for their spatial data assistances. Works on this article has benefited from the financial support of the National Natural Science Foundation of China (Grant No. 40771192) and ITC in the Netherlands.

## References

- Abbaspour, C. Karim, Yang, Jing, Maximov, Ivan, Siber, Rosi, Bogner, Konrad, Mieleitner, Johanna, Zobrist, Juerg, Srinivasan, Raghavan, 2007. Modelling hydrology and water quality in the pre-alpine/alpine Thur watershed using SWAT. *Journal of Hydrology* 333 (2–4), 413–430.
- Ahearn, S. Dylan, Sheibley, W. Richard, Randy, A. Dahlgren, Anderson, Michael, Johnson, Joshua, Tate Kenneth, W., 2005. Land use and land cover influence on water quality in the last free-flowing river draining the western Sierra Nevada, California. *Journal of Hydrology* 313 (3–4), 234–247.
- Arnold, J.G., Muttiah, R.S., Srinivasan, R., Allen, P.M., 2000. Regional estimation of base flow and groundwater recharge in the Upper Mississippi river basin. *Journal of Hydrology* 227 (1–4), 21–40.
- Arnold, J.G., Srinivasan, R., Muttiah, R.S., Williams, J.R., 1998. Large area hydrologic modeling and assessment Part I: model development. *Journal of the American Water Resources Association* 34 (1), 73–89.
- Azzellino, A., Salvetti, R., Vismara, R., Bonomo, L., 2006. Combined use of the EPA-QUAL2E simulation model and factor analysis to assess the source apportionment of point and non point loads of nutrients to surface waters. *Science of The Total Environment* 371 (1–3), 214–222.
- Behera, S., Panda, R.K., 2006. Evaluation of management alternatives for an agricultural watershed in a sub-humid subtropical region using a physical process based model. *Agriculture, Ecosystems & Environment* 113 (1–4), 62–72.
- Bouldin, J.L., Farris, J.L., Moore, M.T., Cooper, C.M., 2004. Vegetative and structural characteristics of agricultural drainages in the Mississippi Delta landscapes. *Environmental Pollution* 132 (3), 403–411.
- Brunsell, N.A., 2006. Characterization of land-surface precipitation feedback regimes with remote sensing. *Remote Sensing of Environment* 100 (2), 200–211.
- Chang, HeeJun, 2008. Spatial analysis of water quality trends in the Han River basin, South Korea. *Water Research* 42 (13), 3285–3304.
- Chaplot, V., 2005. Impact of DEM mesh size and soil map scale on SWAT runoff, sediment, and NO<sub>3</sub>-N loads predictions. *Journal of Hydrology* 312 (1–4), 207–222.
- Feng, J.M., Wang, T., Qi, S.Z., Xie, C.W., 2005. Land degradation in the source region of the Yellow River, northeast Qinghai-Xizang Plateau: classification and evaluation. *Environmental Geology* 47 (4), 459–466.
- Flipo, Nicolas, Jeannée, Nicolas, Poulin, Michel, Even, Stéphanie, Ledoux, Emmanuel, 2007. Assessment of nitrate pollution in the Grand Morin aquifers (France): combined use of geostatistics and physically based modeling. *Environmental Pollution* 146 (1), 241–256.
- George, N., Zaimes, Richard, C., Schultz, Thomas, M., Isenhardt, 2008. Total phosphorus concentrations and compaction in riparian areas under different riparian land-uses of Iowa. *Agriculture, Ecosystems & Environment* 127 (1–2), 22–30.
- Gowda, H. Prasanna, Mulla, J. David, Jaynes, B. Dan, 2008. Simulated long-term nitrogen losses for a midwestern agricultural watershed in the United States. *Agricultural Water Management* 95 (5), 616–624.
- Haregeweyn, Nigussie, Yohannes, Fekadu, 2003. Testing and evaluation of the agricultural non-point source pollution model (AGNPS) on Augucho catchment, western Hararghe, Ethiopia. *Agriculture, Ecosystems & Environment* 99 (1–3), 201–212.
- Krause, Stefan, Jacobs, Joerg, Voss, Anja, Bronstert, Axel, Zehe, Erwin, 2008. Assessing the impact of changes in landuse and management practices on the diffuse pollution and retention of nitrate in a riparian floodplain. *Science of The Total Environment* 389 (1), 149–164.
- Maillard, Philippe, Santos, Nádia Antônia Pinheiro, 2008. A spatial-statistical approach for modeling the effect of non-point source pollution on different water quality parameters in the Velhas river watershed—Brazil. *Journal of Environmental Management* 86 (1), 158–170.
- Merrill, A.G., Benning, T.L., 2006. Ecosystem type differences in nitrogen process rates and controls in the riparian zone of a montane landscape. *Forest Ecology and Management* 222 (1–3), 145–161.
- Misgana, K. Muleta, John, W. Nicklow, 2005. Sensitivity and uncertainty analysis coupled with automatic calibration for a distributed watershed model. *Journal of Hydrology* 306 (1–4), 127–145.
- Ning, Shukuang, Chang, Nibin, Jeng, Kaiyu, 2006. Soil erosion and non-point source pollution impacts assessment with the aid of multi-temporal remote sensing images. *Journal of Environmental Management* 79 (1), 88–101.
- Oki, Kazuo, Yasuoka, Yoshifumi, 2008. Mapping the potential annual total nitrogen load in the river basins of Japan with remotely sensed imagery. *Remote Sensing of Environment* 112 (6), 3091–3098.
- Ouyang, Wei, Hao, Fanghua, Wang, Xuelei, Cheng, Hongguang, 2008a. Non point source pollution responses simulation for conversion cropland to forest in mountains by SWAT in China. *Environmental Management* 41 (1), 79–89.
- Ouyang, Wei, Hao, Fanghua, Wang, Xuelei, 2008b. Regional non point source organic pollution modeling and critical area identification for watershed best environmental management. *Water, Air, & Soil Pollution* 187 (1–4), 251–261.
- Pontus, Olofsson, Lars, Eklundh, Fredrik, Lagergren, Per, Jönsson, Anders, Lindroth, 2007. Estimating net primary production for Scandinavian forests using data from Terra/MODIS. *Advances in Space Research* 39 (1), 125–130.
- Stefanov, L. William, Netzband, Maik, 2005. Assessment of ASTER land cover and MODIS NDVI data at multiple scales for ecological characterization of an arid urban center. *Remote Sensing of Environment* 99 (1–2), 31–43.
- Vicente Serrano, S.M., Cuadrat Prats, J.M., Romo, A., 2006. Aridity influence on vegetation patterns in the middle Ebro Valley (Spain): evaluation by means of AVHRR images and climate interpolation techniques. *Journal of Arid Environments* 66 (2), 353–375.
- Wang, Genxu, Shen, Yongping, Cheng, Guodong, 2000. Eco-environmental changes and causal analysis in the source regions of the yellow river. *Journal of Glaciology and Geocryology* 22 (3), 200–205.
- Wang, Xiaodan, Li, MaiHe, Liu, Shuzhen, Liu, Gangcai, 2006. Fractal characteristics of soils under different land-use patterns in the arid and semiarid regions of the Tibetan Plateau, China. *Geoderma* 134 (1–2), 56–61.
- Wardlow, D. Brian, Egbert, L. Stephen, 2008. Large-area crop mapping using time-series MODIS 250 m NDVI data: an assessment for the U.S. Central Great Plains. *Remote Sensing of Environment* 112 (3), 1096–1116.
- William, L. Stefanov, Maik, Netzband, 2005. Assessment of ASTER land cover and MODIS NDVI data at multiple scales for ecological characterization of an arid urban center. *Remote Sensing of Environment* 99 (1–2), 31–43.
- Williams, J.R., 1995. Chapter 25. The EPIC Model. In: *Computer Models of Watershed Hydrology*. Water Resources Publications, Highlands Ranch, CO, pp. 909–1000.
- Wu, Yuhu, 2004. The vegetation types and its characteristics of natural grassland in the source area of yellow river. *Chinese Journal of Grassland* 26 (2), 70–75.
- Xian, George, Crane, Mike, Su, Junshan, 2007. An analysis of urban development and its environmental impact on the Tampa Bay watershed. *Journal of Environmental Management* 85 (4), 965–976.
- Yang, Shengtian, Cheng, Hongguang, Bu, Qingsong, Zhang, Jianyong, Shi, Xiaoxin, 2006. Estimation of soil erosion and its application in assessment of the absorbed nitrogen and phosphorus load in China. *Acta Scientiae Circumstantiae* 26 (3), 366–374.
- Yuan, D., Lin, B., Falconer, R.A., Tao, J., 2007. Development of an integrated model for assessing the impact of diffuse and point source pollution on coastal waters. *Environmental Modelling & Software* 22 (6), 871–879.
- Zhang, Na, He, Dawei, Chen, Jingshen, Cui, Shubin, 2003. A preliminary study on nitrogen contamination in the Yellow River system, China. *Environmental Chemistry* 2 (22), 105–110.